Synthesis of biomass derived levulinate esters on novel sulfated Zr/ KIL-2 composite catalysts

Margarita Popova[a*], Agnes Szegedi[b], Hristina Lazarova[a] , Alenka Ristić[c], Yuri Kalvachev[d],

Genoveva Atanasova[e], Nicole Wilde[f], Natasa Novak Tusar [c,g], Roger Gläser[f]

[a]Institute of Organic Chemistry with Centre of Phytochemistry, Bulgarian Academy of Science, 1113 Sofia, Bulgaria
[b]Research Centre for Natural Sciences, Hungarian Academy of Sciences, Institute of Materials and Environmental Chemistry, 1117 Budapest, Magyar tudósok körútja 2, Hungary
[c]National Institute of Chemistry Slovenia, Hajdrihova 19, 1001 Ljubljana, Slovenia
[d]Institute of Mineralogy and Crystallography, Bulgarian Academy of Sciences, 1113 Sofia, Bulgaria
[e]Institute of General and Inorganic Chemistry, Bulgarian Academy of Sciences, 1113 Sofia, Bulgaria
[f]Universität Leipzig, Institute of Chemical Technology, Linnestr. 3, 04103 Leipzig, Germany
[g]University of Nova Gorica, Vipavska 13, 5001 Nova Gorica, Slovenia

 *Corresponding author. Margarita Popova, Institute of Organic Chemistry with Centre of Phytochemistry, Acad. G. Bonchev str., bl.9, 1113 Sofia, Bulgaria.
 E-mail address: mpopova@orgchm.bas.bg (M. Popova).

Abstract

Zirconia nanomaterials were prepared by impregnation of KIL-2 type silica with 4, 8, 15 and 25 wt% of ZrO_2, and were modified by sulfate groups in order to vary the type, strength and density of the active sites. The samples were characterized by X-ray powder diffraction (XRD), EDX analysis, N_2 physisorption, SEM, TEM, UV-Vis spectroscopy, XPS, and thermogravimetric analysis (TGA). The acidic properties were investigated by FT-IR spectroscopy of adsorbed pyridine. The catalytic properties of ZrKIL-2 catalysts and their sulfated varieties were studied in levulinic acid (LA) esterification with ethanol or n-butanol. The sulfated materials showed significantly higher activity compared to the non-sulfated ones due to their stronger Brönsted and Lewis acid sites. It was found that the silica supported sulfated samples show different activity depending on the applied alcohol. With increasing ZrO_2 content up to 15 wt% increasing catalytic activity and selectivity was observed to produce levulinate esters. A further increase of the amount of zirconia leads to a decrease in catalytic activity because of the significant decrease of ZrO_2 dispersion and the structure deterioration of the catalyst. For the first time insight was provided into the relation between sulfates group leaching and zirconia dispersion.

1.   Introduction

The utilization of lignocellulosic biomass to produce chemicals, fuels and energy has gained considerable attention in recent years due to the decrease of fossil fuel resources and the increase in energy consumption. Levulinic acid and its esters are promising platform chemicals for the production of a broad range of sources for the biofuel, polymer and fine chemicals industry [1-5]. Levulinic acid (LA) is generally produced by the acid-catalyzed hydro- lysis of cellulose, and can be converted into levulinate esters, γ-valerolactone, 1,4-pentanediol and 5-nonanone (via pentanoic acid) as well as diphenolic acid as an intermediate for the synthesis of epoxy resins and poly-carbonates [6-10]. Levulinate esters are also valuable compounds that can be used as fuel additives, sol- vents and plasticizers. In particular, ethyl levulinate can directly be used up to 5 wt% as a diesel miscible biofuel in regular diesel engines without modification because of its physicochemical properties similar to those of biodiesel, i.e., fatty acid methyl esters (FAME) [6]. Therefore it has the potential to decrease the consumption of petroleum-derived fossil fuels. Generally, levulinate esters are produced by esterification of LA with several alcohols using mineral acids such as HCl, H_2SO_4 and H_3PO_4 as catalysts, resulting in the high yield of corresponding products within a short reaction time. However, such soluble acid catalysts cannot be recycled and always lead to technological problems (e.g., use of a large volume of base for neutralization and corrosion of equipment). The replacement of homogeneous catalysts with heterogeneous analogues which are easily separable and reusable is thus highly desirable.

Esterification of LA with alcohols, such as ethanol or n-butanol (Scheme 1), occurs even at room temperature, but the reaction is very slow and needs to be sped up either by using a high temper- ature (70e100 C) or by using a catalyst to achieve the equilibrium conversion in a timely way [11-19].
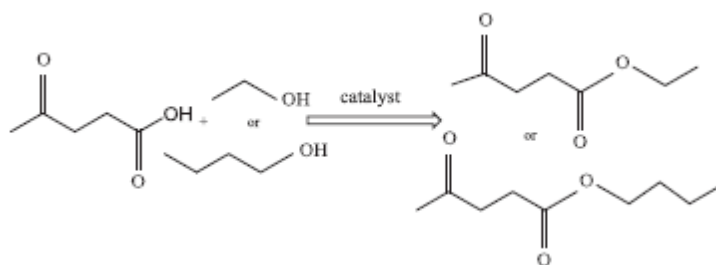
Scheme 1.

Various solid acids have been used for the esterification of levulinic acid with alcohols, e.g., zeolites and sulfated mixed oxides (sulfated zirconia (SO_4^{2-}/ZrO_2), niobia (SO_4^{2-}/Nb_2O_5), titania (SO_4^{2-}/TiO_2) and stannia (SO_4^{2-}/SnO_2) [9,20-23]. Among them, the sulfated mixed oxides with strong acid sites are the most promising candidates providing high catalytic activity in a suitable reaction time [4]. The number and the strength of acid sites and the applied preparation conditions are the key parameters for the catalysts activity. Optimizing the preparation

conditions, the density of acid sites and the dispersion state of the sulfate species can lead to further improvements of the activity of the sulfated mixed oxides. One possible strategy is the introduction of mesopores in the mixed oxides via a surfactant induced self-assembly approach [24,25]. Another solution is the fine dispersion of active oxide phase on an appropriate neutral, high surface area support, e.g., mesoporous silica materials [26-28]. The resulting high surface area provides higher dispersion and an increased density of the acid sites. Both methods can enhance the catalytic activity of such materials in liquid-phase reactions by accelerating mass transport of the reactant and product molecules. We expect that the nanosized KIL-2 material with textural mesoporosity could provide the opportunity for high dispersion of the modifier because of the high surface area and better diffusion of the reactants to the active sites and the products out of the larger pores.

In the present study ZrO_2 deposited on KIL-2 material, functionalized by sulfate groups was studied and compared in the levulinic acid esterification with ethanol and n-butanol. The influence of the textural characteristics of the mesoporous KIL-2 support, ZrO_2 content and the type of the formed acidic sites on the activity to produce levulinate esters is discussed.

2. Experimental

2.1. Material preparation

2.1.1. KIL-2 synthesis

In the first step, the silica source (tetraethyl orthosilicate, 98% TEOS, Acros) as well as the templates (triethanol amine (99% TEA, Fluka), tetraethylammonium hydroxide (20% TEAOH, Acros)) were mixed with a molar composition of 1.0 TEOS: 0.5 TEA: 0.1 TEAOH: 11 H_2O to obtain a homogeneous gel. The gel was aged overnight at room temperature and then dried in an oven for 24 h at 50°C. In the second step, the gel was solvothermally treated in ethanol in Teflon-lined stainless steel autoclaves at 150°C for 48 h. Removal of the template was performed by calcination at 500°C for 10 h using a ramp rate of 1°C/min in air flow.

2.1.2. Functionalization of KIL-2 by ZrO_2

An incipient wetness impregnation technique with $ZrCl_2$ (99%, Aldrich) was applied for loading of 4, 8, 15 and 25 wt% metal oxide. In a typical experiment 1 g of KIL-2 was mixed with 1 ml aqueous solution of $ZrCl_2$ at room temperature. The precursor salt was decomposed in air at 500 C for 2 h for all samples. Samples were designated as xZrKIL-2 where x = 4, 8, 15 and 25 wt% ZrO_2.

2.1.3. Functionalization of Zr/KIL-2 by SO_4^{2-} groups

ZrKIL-2 samples were mixed with 10% H_2SO_4 solution (40 ml/1 g ZrO_2) at room temperature for 2 h. The suspension was dried at ambient and calcined at 500°C for 3 h. Samples were designated as SO_4^{2-}/xZrKIL-2 where x = 4, 8, 15 and 25 wt% ZrO_2.

2.2. Characterization

The X-ray powder diffraction (XRD) patterns were recorded on a PANalytical X'Pert PRO (HTK) high-resolution diffractometer using Cu Ka$_1$ radiation (1.5406 E) in the 2 θ range from 5 to 80 (100 s per step 0.016) for the samples and from 10 to 80 (100 s per step 0.016) for the sample holder using a fully opened X'Celerator detector.

Nitrogen physisorption measurements were carried out at -196 °C using Tristar 3000 Micromeritics volumetric adsorption analyzer. Before the adsorption analysis, the samples were outgassed under vacuum for 2 h at 200 °C in the port of the adsorption analyzer. The BET specific surface area was calculated from adsorption data in the relative pressure range from 0.05 to 0.21 [29]. The total pore volume was estimated on the basis of the amount adsorbed at a relative pressure of 0.96 [30]. The mesopore and micropore volumes were determined using the t-plot method [31]. The pore size distributions (PSDs) were calculated from nitrogen adsorption data using an algorithm based on the ideas of Barrett, Joyner, and Halenda (BJH) [32]. The mesopore diameters were determined as the maxima on the PSD for the given samples.

FT-IR experiments were performed with Nicolet Compact 640 spectrometer by the self-supported wafer technique with pyridine (Py) (7 mbar) as probe molecule. Self-supported pellets (10 20 mm) were pressed from the samples, placed into the IR cell, heated up to 350 °C in high vacuum (106 mbar) with a rate of 10 °C/min and dehydrated for 1 h. Following 30 min contact with Py at 100 °C the sample was evacuated subsequently at 100, 200, 300, and 400 °C for 30 min. After each evacuation step a spectrum was recorded at IR beam temperature with a resolution of 2 cm^{-1}. The spectra were normalized to 5 mg/cm^2 weight of the wafers for comparison.

Scanning electron micrographs (SEM) were taken on electron microscope Zeiss SupraTM 3VP microscope. Elemental analysis of all samples was performed by energy dispersive X-ray analysis (EDX) with an INCA Energy system attached to a Zeiss SupraTM 3VP microscope.

TEM images were taken using a MORGAGNI 268D TEM (100 kV; W filament; 153 point-resolution =0.5 nm).

The composition and the chemical properties of the selected samples were analyzed by X-ray photoelectron spectroscopy (XPS). The measurements were carried out on AXIS Supra electron- spectrometer (Kratos Analytical Ltd.) using monochromatic AlK$_a$ radiation with photon energy of 1486.6 eV. The energy calibration was performed by normalizing the C1s line of adsorbed adventitious hydrocarbons to 284.6 eV. The binding energies (BE) were determined with an accuracy of ±0.1 eV. The chemical composition of the samples was determined monitoring the areas and binding energies of O1s, Si2p, Zr3d and S2p photoelectron peaks. Using the commercial data-processing software of Kratos Analytical Ltd. the concentrations of the different chemical elements (in atomic %) were calculated by normalizing the areas of the photoelectron peaks to their relative sensitivity factors.

The thermogravimetric analysis (TGA) was performed with DTA-TG analyzer SETSYS2400, SETARAM under the following conditions: temperature range 25-100°C, static air atmosphere, heating rate of 5 °C/min.

2.3. Catalytic experiments

Prior to the catalytic experiments, the materials were pretreated ex-situ for 1 h at 140 °C in static conditions at ambient air. A batch reactor with magnetic stirrer was used to perform the esterification reaction. In a typical experiment, the reactor was charged with 2 g LA and 0.050 g powder catalyst (2.5 wt% catalyst/LA), LA/ethanol or n-butanol weight ratio was 1:5. The reactor was heated to the desired reaction temperature (70-100°C) for 1 h. The analysis of the reaction products was performed using HP-GC with FID and a WCOT FUSED SILICA 25 m 0.25 mm COATING CP-SIL 43CB column. The mass balance is made on the basis of carbon-containing products.

3. Results and discussion

3.1. Physico-chemical properties

XRD patterns of the studied catalysts are shown in Fig. 1. 4ZrKIL- 2 and 8ZrKIL-2 samples possessing 4 and 8 wt% zirconia, respectively do not show detectable diffraction peaks that could be assigned to zirconia phases. This means that either such oxides are not present within KIL-2 samples or that their crystallites are very small with typical dimensions of 5 nm or less and thus they are not detectable by XRD. The same phenomenon can be observed on sulfated analogues of 4ZrKIL-2 and 8ZrKIL-2.

Impregnated KIL-2 samples with 15 and 25 wt% of zirconia show the presence of crystalline monoclinic ZrO_2 phase (Badelleyit, PDF 01-083-944). The XRD pattern of sulfated 15Zr/KIL-2 indicates the presence of monoclinic zirconia, whereas the sulfated analogue of 25 wt% of zirconia contains a mixture of monoclinic ZrO_2, tetragonal ZrO_2 (PDF 01-089-6976), zirconium sulfate (PDF 00-020-1474) and its tetrahydrate form (PDF 04-011-5222). According to the intensity change of the monoclinic ZrO_2 phase after sulfation, about one third of the initial zirconia content remains unsulfated on 25Zr/ KIL-2.

Nitrogen adsorption isotherms for ZrKIL-2 samples and their sulfated analogues are shown in Fig. 2, and textural parameters determined by the isotherms are listed in Table 1. All the samples exhibit adsorption isotherms of IV type typical of KIL silicas, with a relatively narrow hysteresis loop. All hysteresis loops of samples containing ZrO_2 are less intensive in comparison to the original support. Impregnation of the support with lower amounts of zirconia (4-8 wt%) resulted in a decrease of surface area and pore volume and an increase of pore diameter. Higher amounts of loaded ZrO_2 on KIL-2 (25 wt %) led to much lower specific surface area (139 m^2/g),
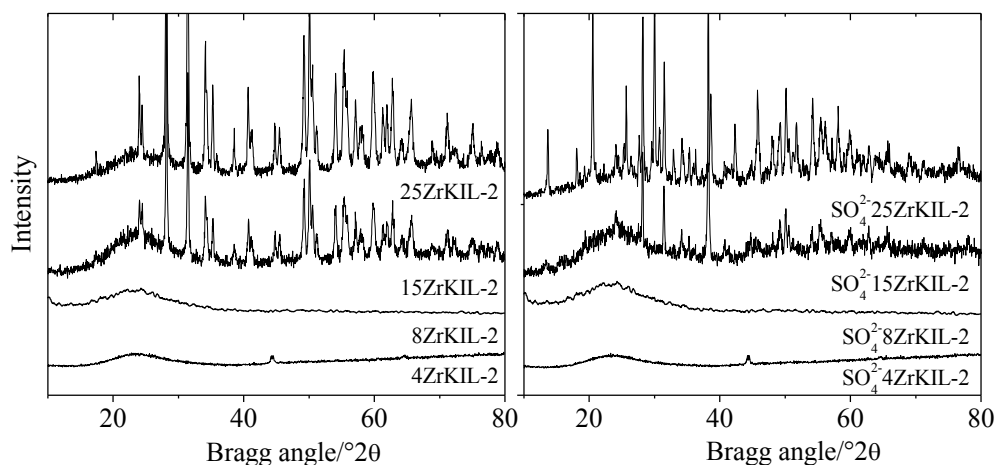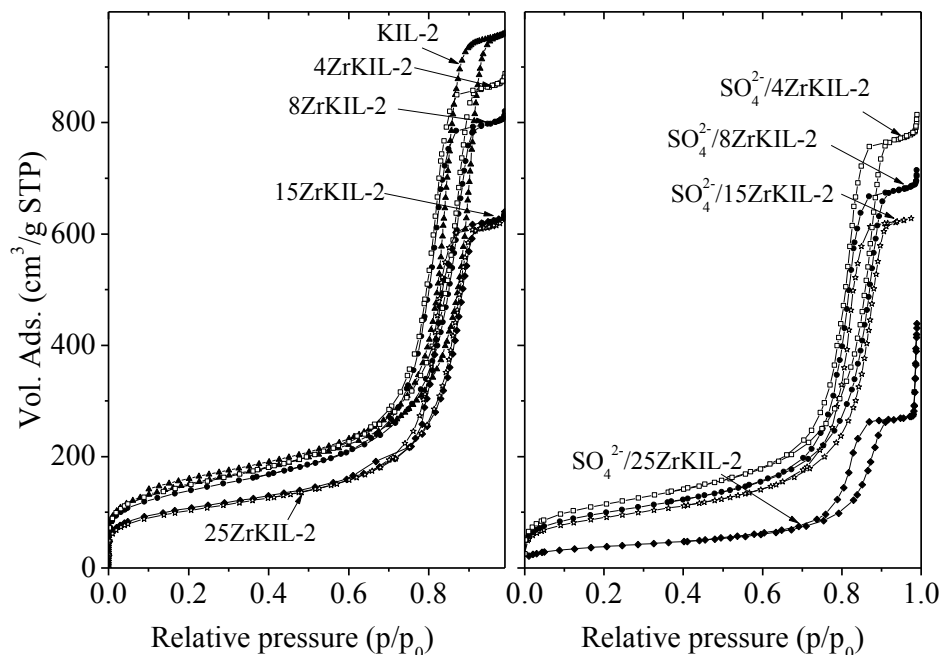
Fig. 1. XRD patterns of the studied samples

pore volume (0.42 cm^3/g) and an increased average pore diameter (16.6 nm) (Table 1). The second step on the desorption branch due to the existence of ZrO$_2$ nanoparticles in mesopores is evidenced for the 25ZrKIL2 sample, whereas for all other samples the second-step is not observed. The reason could be that pore blocking was avoided by the formation of smaller ZrO$_2$ nanoparticles in these samples than in the 25ZrKIL2 sample.

Zirconia nanoparticles are immobilized in the silica matrix due to the interaction with the silanol groups on the surface which was evidenced in the FTIR spectra of the samples in the silanol region (not shown). It can also be observed that sulfated ZrKIL-2 samples undergo a capillary condensation step at higher relative pressures than the non-sulfated analogues, indicating that larger mesopores are present in the sulfated samples. This effect can be explained by some destruction of the mesostructured pore system, caused by the corrosive action of sulfuric acid, resulting in some dissolution of silica [33].

Table 1 Textural properties of the studied samples determined by N$_2$ physisorption.

| Samples	S_{BET} (m^2/g)	V_{tot} (cm^3/g)	V_{meso} (cm3/g)	V_{micro} (cm3/g)	S_{meso} (m2/g)	S_{ext} (m2/g)	Pore diameter (nm)
KIL-2	664	1.45	1.29	0.07	464	57	15.2
4ZrO2/KIL-2	525	1.34	1.20	0.01	354	52	15.7
SO$_4^{2-}$/4ZrKIL-2	408	1.20	1.07	0.02	280	61	16.2
8ZrO2/KIL-2	494	1.24	1.11	0.05	330	45	15.7
SO$_4^{2-}$/8ZrKIL-2	355	1.06	0.95	0.02	249	31	16.2
15ZrKIL-2	385	0.96	0.86	0.04	250	36	15.7
SO$_4^{2-}$/15ZrKIL-2	328	0.96	0.88	0.02	232	39	16.6
25ZrKIL-2	371	0.95	0.85	0.03	236	51	15.9
SO$_4^{2-}$/25ZrKIL-2	139	0.42	0.36	-	88	29	16.6
SO$_4^{2-}$/4ZrKIL-2(U)	361	1.09	1.00	-	309	52	15.0
SO$_4^{2-}$/15ZrKIL-2(U)	224	0.68	0.60	-	179	44	15.2
SO$_4^{2-}$/25ZrKIL-2(U)	270	0.81	0.69	-	198	72	15.4

*U-spent catalyst.

**Fig. 2.** Nitrogen adsorption/desorption isotherms of ZrKIL-2 catalysts, and their sulfated analogues

Upon modification with 25 wt% of zirconia the surface a rea and the pore volume do not change significantly compared to other samples, however after functionalization with sulfuric acid these textural properties decrease significantly, approximately to the half of the non-sulfated one. This effect can be explained by the formation of a separate crystalline zirconia sulfate phase influencing the mesopore structure [27].

Fig. 3 shows the DR UV-vis spectra recorded in the region between 200 and 400 nm of Zr-modified KIL-2 samples and their sulphated analogs. The absorption band observed at 206 nm in the spectra of KIL-2 samples modified with 4 and 8 wt% ZrO_2 (Fig. 3) is attributed to the presence of monodispersed Zr atoms surrounded by four oxygen bridged silicon atoms in the silica matrix [15,24,27]. The intensive peak at 235 nm is typical of bulk crystalline ZrO_2, whereas the absorption band at around 300 nm is due to the for- mation of small nanosized ZrO_2 particles [15,24,27]. The latter has the highest intensity for the sulfated 15ZrKIL-2 and 25ZrKIL-2 samples (Fig. 3). The sulfating process leads to a redispersion of the zirconium oxide phase, which is in good accordance with the XRD results.

TG/DTG plots of the sulfated ZrKIL-2 samples are shown in Fig. 4. The weight loss registered at temperatures above 600°C is due to the decomposition of SO_4^{2-} groups. TG curves of all samples show two peaks with maxima at 700°C and 800°C related to the SO_4^{2-} decomposition. The TG profiles of sulfated 15ZrKIL-2 and 25ZrKIL-2 samples show similar weight loss (≈ 8 wt %) but the temperature for decomposition of sulfated groups is shifted by 35°C to higher for
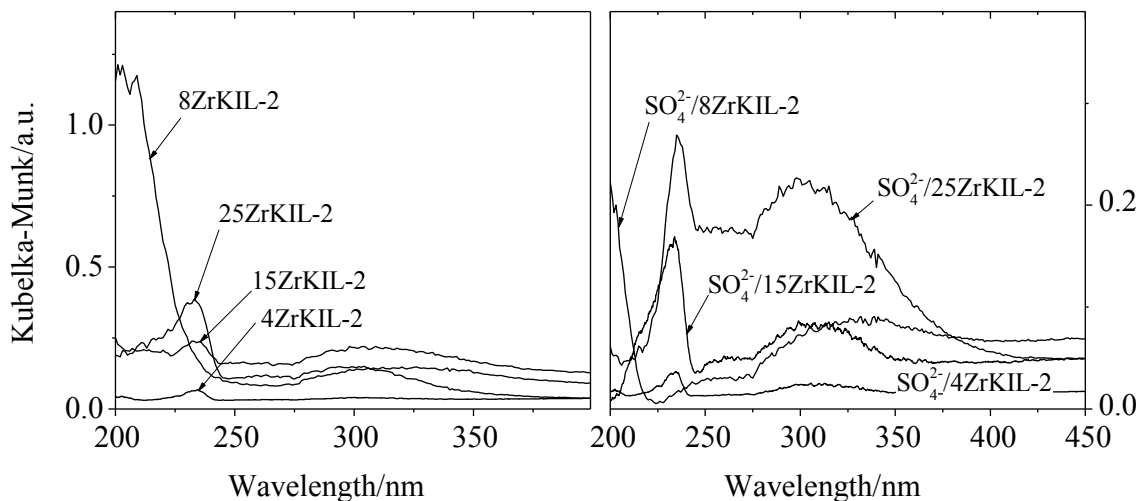
Fig. 3. UV-Vis spectra of the studied samples.
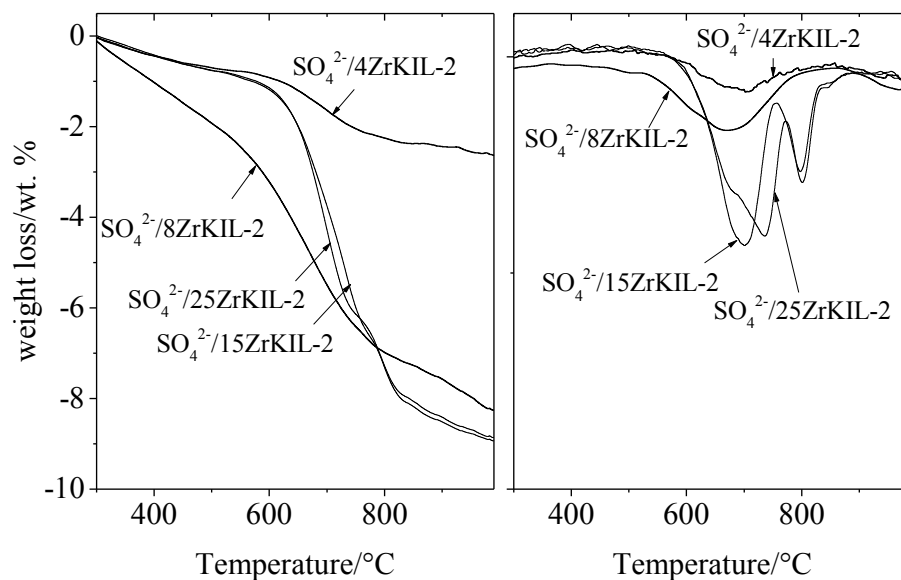

Fig. 4. TGA of the studied samples.

the $SO_4^{2-}/25ZrKIL-2$ sample. Sulfate content of $SO_4^{2-}/4ZrKIL-2$ and $SO_4^{2-}/8ZrKIL-2$ samples (Table 1) is much lower than in the $SO_4^{2-}/15ZrKIL-2$ and $SO_4^{2-}/25ZrKIL-2$ samples. It seems that modification with 15 wt% zirconia is the optimal composition to achieve the highest sulfate content during the sulfating procedure. The XRD data also confirm that the sulfation is incomplete for the $SO_4^{2-}/25ZrKIL-2$ sample.

Table 2 Composition of the sulfated ZrKIL-2 samples.

Samples	SO_4^{2-} content (wt.%)	Sulfate groups leaching, %	O, (at. %)	Si, (at. %)	S, (at. %)	Zr, (at. %)	S/Zr
SO_4^{2-}/4ZrKIL-2	1.9	-	70.4	28.7	0.4	0.5	0.8
SO_4^{2-}/8ZrKIL-2	5.6	-	70.3	28.7	0.6	0.5	1.2
SO_4^{2-}/15ZrKIL-2	7.9	-	70.7	26.7	1.0	1.5	0.7
SO_4^{2-}/25ZrKIL-2	8.0	-	72.7	23.0	1.5	2.8	0.5
SO_4^{2-}/4ZrKIL-2(U)	1.7	10.5	70.2	28.7	0.6	0.5	1.2
SO_4^{2-}/8ZrKIL-2(U)	5.0	10.7	70.3	28.1	0.7	0.8	0.9
SO_4^{2-}/15ZrKIL-2(U)	7.5	5.1	71.0	26.2	1.1	1.6	0.7
SO_4^{2-}/25ZrKIL-2(U)	6.8	15.0	77.9	19.0	0.6	2.4	0.3

*U spent catalyst.
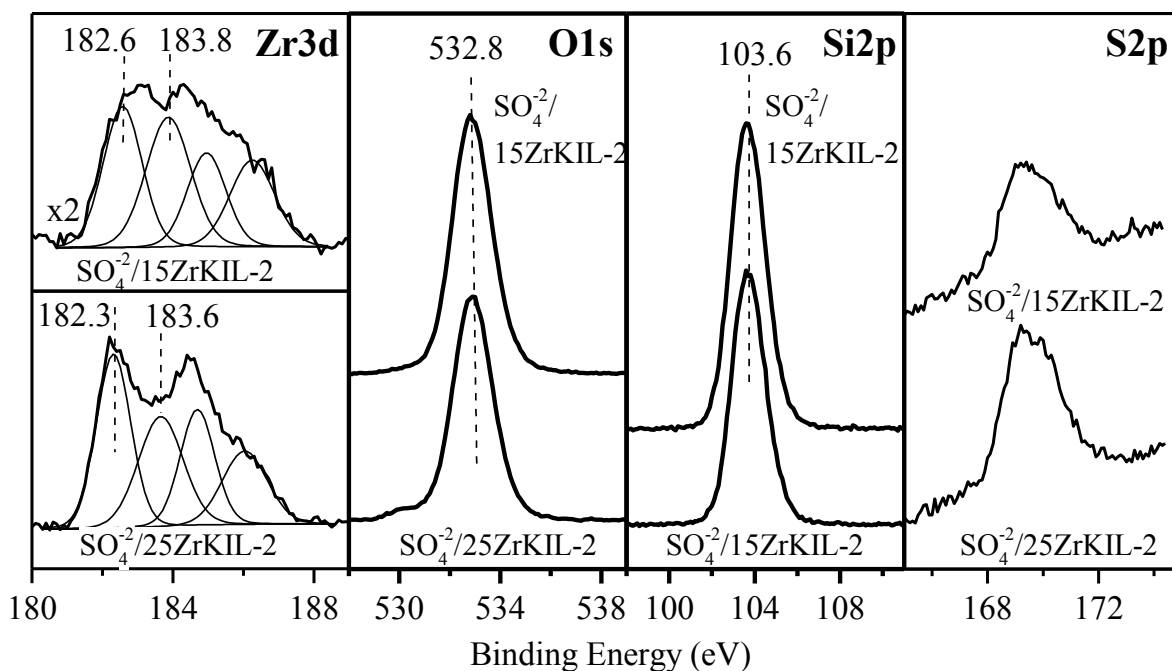
Fig. 5. Zr 3d, O 1s and Si 2p and S 2p XPS regions of the SO_4^{2-}/15ZrKIL-2 and SO_4^{2-}/25ZrKIL-2 samples

The chemical compositions of the catalysts determined by EDX are presented in Table 2. The increase of the sulfur content is registered with zirconium content increase for the sulfated Zr/KIL-2 samples. The zirconium precursor was decomposed completely during the calcination step and the presence of chloride anions was not registered in all studied samples. The calculated S/Zr ratio for the SO24/25ZrKIL-2 sample is an indication that a significant part of zirconia is not sulfated, which is in good accordance with the XRD and TGA results.

The surface chemical compositions of the $SO_4^{2-}/15ZrKIL-2$ and $SO_4^{2-}/25ZrKIL-2$ samples were additionally explored by XPS. Complex shapes were observed for the zirconium 3d spectral regions (Fig. 5) which can be fitted with two pairs of Zr 3d5/2 and Zr 3d3/2 peaks with a characteristic spine orbital splitting of 2.4 eV. The sulfation procedure influences the intensity ratio of both Zr 3d pairs for the 15ZrKIL-2 and 25ZrKIL-2 samples (Fig. 5, Table 3). The lower Zr 3d5/2 binding energy at 182.3 eV is in the range of Zr(IV) in ZrO2, whereas the higher energy component at 183.6 eV corresponds to the formation of Zr(IV) species bound to more electron attractive species, despite not being relative to $ZrSO_4$ [25,26,28]. The higher intensity of the Zr 3d5/2 peak detected for $SO_4^{2-}/25ZrKIL-2$ is in agreement with the XRD data showing the crystalline ZrO_2 formation. The O ls peak centered around 532.0 eV can be attributed to oxygen atoms from silica as well as OH and/or sulfates groups [26,28,34]. A small peak centered at around 530.0 eV in O 1s XP spectrum of $SO_4^{2-}/25ZrKIL-2$ is assigned to the oxygen atoms from the zirconia framework. Furthermore S2p peak centered at 169.2 eV is characteristic of sulfates species. The sulfate surface content (Zr/S ratio) is higher for the $SO_4^{2-}/25ZrKIL-2$ sample compared to that of the $SO_4^{2-}/15ZrKIL-2$ sample (Table 3), whereas the determined amount of sulfate content by TG analysis is equal for both samples. This effect could be due to the higher crystallinity of ZrO2 formed on the $SO_4^{2-}/25ZrKIL-2$ sample than that of on the SO24/15ZrKIL-2 sample. Also the predominant distribution of sulfate groups on the outer surface of the $SO_4^{2-}/25ZrKIL-2$ sample and in the channels of the $SO_4^{2-}/15ZrKIL-2$ sample can contribute to this phenomenon.

Table 3
Composition of SO24/15ZrKIL-2 and SO24/25ZrKIL-2 samples derived from XPS.

Samples	Si/Zr	Zr/S	S	Zr	Zr 3d (182.3eV)	Zr 3d (183.6 eV)	Si	O
			(at. %)	(at. %)	(at. %)	(at. %)	(at. %)	(at. %)
$SO_4^{2-}/25ZrKIL-2$	13.3	1.1	1.8	2.0	54.8	45.2	26.5	69.7
$SO_4^{2-}/15ZrKIL-2$	22.4	1.6	0.8	1.3	48.5	51.5	29.1	68.8

3.2.Characterization of the acid site density, strength and nature by FT-IR spectroscopy of adsorbed pyridine

Zirconia and sulfated zirconia materials possess acid sites, i.e. Lewis and Brönsted acid surface sites can be distinguished. The relative amount and nature of these types of acidic species can be determined by FT-IR spectroscopic investigation of adsorbed pyridine (Py) [35-39]. Lewis acid sites can be associated with the ring vibrations of coordinatively bound Py at 1610 and 1448 cm^{-1} (Py-L) [34-38]. The weak bands at 1446 cm^{-1}, appearing as a shoulder of the 1448 cm^{-1} band and its pair at 1598 cm^{-1}, are assigned to hydrogen-bonded Py with the silanolic OH groups. Only the presence of Lewis acid sites is registered on non-sulfated samples (not shown), originating from coordinatively unsaturated Zr ions on the surface of the support. Higher amount of Zr
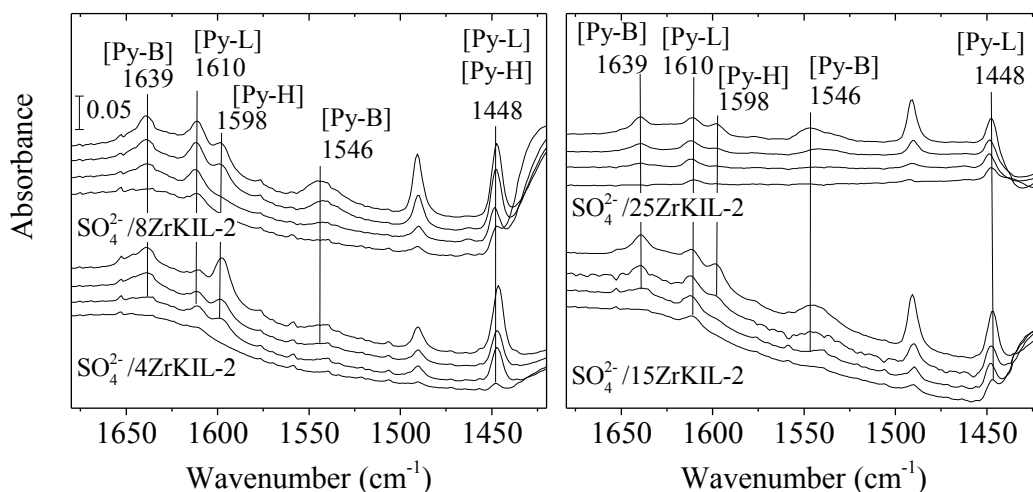
Fig. 6. FT-IR spectra of adsorbed pyridine on sulfated ZrKIL-2 samples with 4, 8, 15 and 25 wt% of zirconia. Self-supported pellets were pretreated at 350°C in vacuum and contacted with Py (7 mbar) for 30 min. Spectra were collected after Py desorption at 100, 200, 300 and 400°C for 30 min, shown from top to bottom for each sample.

loading leads to a small increase of the amount of Lewis acid sites. However, loading of 25 wt% of zirconia resulted in a significant decrease of the Lewis acid sites, only hydrogen-bonded Py can be seen on its FT-IR spectra. It seems that with the highest amount of zirconia (25 wt %) unreacted silanols remain on the silica carrier. According to XRD results the majority of loaded zirconia in 25ZrKIL-2 exists as a separate oxide phase, and it does not react with the surface of the silica support. Only the 4 wt% zirconia containing sample shows some weak Brönsted acidity due to the formation of zirconia-silica mixed oxide by the 500°C heat treatment in the impregnation procedure. The FT-IR spectra of sulfated samples contain bands characteristic of both Lewis and Brönsted acid sites (Fig. 6). On sulfated zirconia the sulfate species also act as Lewis acid sites, however the presence of the latter increase the Brönsted acid strength of the hydroxyl groups on the surface of zirconia [36]. The protonated Py molecules coordinated to the conjugated base of the solid Brönsted acid (Py-B) exhibit bands at 1546 cm^{-1} and 1639 cm^{-1}. With increasing zirconia content the amount of Lewis acid sites, represented by the intensity of the 1448 cm^{-1} band, is not proportional. Up to 8 wt% the intensities are increasing (Table 4). With further increase of zirconia up to 25 wt% it decreases (Fig. 6). The Brönsted acidity of the sulfated samples with 8 and 15 wt% zirconia is higher than that of 25 wt% and 4 wt% zirconia-containing ones. These facts indicate that there is an optimal zirconia content on the surface, between 8 and 15 wt%, where zirconia can cover the silica support (evidenced from XRD, UV Vis and FTIR data) and no significant separate phase is formed. On the other hand, a low amount of zirconia loading results in the formation of mixed oxide, i.e. surface reaction of zirconium oxide with the silanol groups of the silica support. FT-IR data of Py desorbed at higher

temperature is characteristic for the strength of acid sites of the samples [40]. Integrated intensity data for Py desorbed at 100 and 200°C can be found in Table 4. It can be seen that the amount of B/L ratio decrease at higher temperature but this effect is less pronounced for the SO_4^{2-}/15ZrKIL-2 sample, indicating the presence of high concentration of Brönsted and Lewis acid sites. Investigating the S=O stretching vibration region of the FT-IR spectra, characteristic bands at around 1415 and 1335 cm^{-1} can be found on all samples, except with 4 wt% zirconia, where only the lower frequency band appeared (not shown). According to FT-IR studies of sulfated zirconia bands appearing over 1400 cm^{-1} can be associated with polynuclear, disulfate species, whereas S=O bands at lower frequencies are characteristic of isolated sulfate groups localized on the zirconia crystal plates or on the defects sites [37-40]. The appearance of both types of S=O bands indicate that bigger zirconia particles are formed on samples with higher zirconia content in accordance with the XRD results. Upon Py adsorption only a slight shift to lower wavenumbers was observed of the 1335 cm^{-1} band on 15 and 25 wt% zirconia containing samples. These results support the assumption that in these samples sulfate species can be found in the bulk crystalline phase and only a small part is accessible to Py on the outer surface.
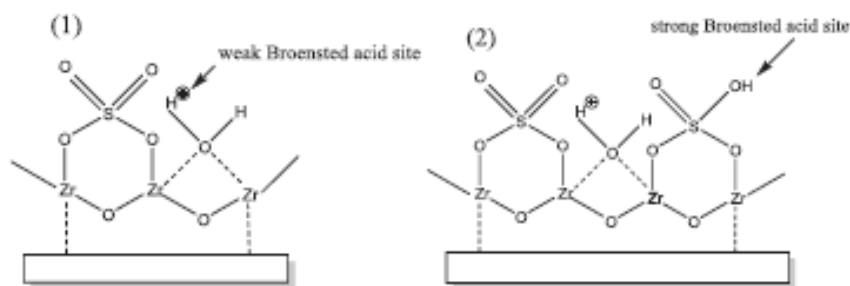

Scheme 2.

Exposure of ZrO2 or Zr(OH)$_4$ surfaces to H$_2$SO$_4$ solutions is suggested to result in surface bisulfate groups (HSO$_4^-$) in a bidentate coordination considering the Clearfield model for acid site formation in sulfated zirconia [24,41,42]. During the subsequent calcination the bisulfate can undergo condensation with adjacent hydroxyl groups to form neutral bidentate sulfate species together with a Lewis acid centre located on the zirconia support. The latter can interconvert to yield weak Brönsted acid sites on coordination with water (Scheme 2, (1)). In the case of the SO_4^{2-}/25ZrKIL-2 sample sulfation is incomplete as it was shown by XRD, TG, EDX and XPS data, and a part of zirconia phase remains not sulfated, leading to the formation of weak Brönsted acid sites.

The high bisulfate coverage of zirconia phase in SO_4^{2-}/15ZrKIL-2 could result in an incomplete condensation reaction during calcination because of insufficient hydroxyl groups. This would result in the stabilization of permanently bound bisulfate Brönsted acid sites as postulated by Clearfield et al. [24] and the generation of new strong acid sites (Scheme 2, (2)). Hence increasing the sulfate loading, and thus the surface bisulfate:hydroxyl ratio, seems to induce a

transition from ZrO_2-derived weak Lewis/Brönsted acid sites in SO_4^{2-}25ZrKIL-2 to bisulfate-derived strong Brönsted acid sites in SO_4^{2-}/15ZrKIL-2.

SEM images are presented in Fig. 7 a-d. Nanoparticles of disordered mesoporous KIL-2 structure with interparticle porosity can be observed in Fig. 7a,b. Additional crystalline phases (oxide/sulfate) can be found in Fig. 7c, d.
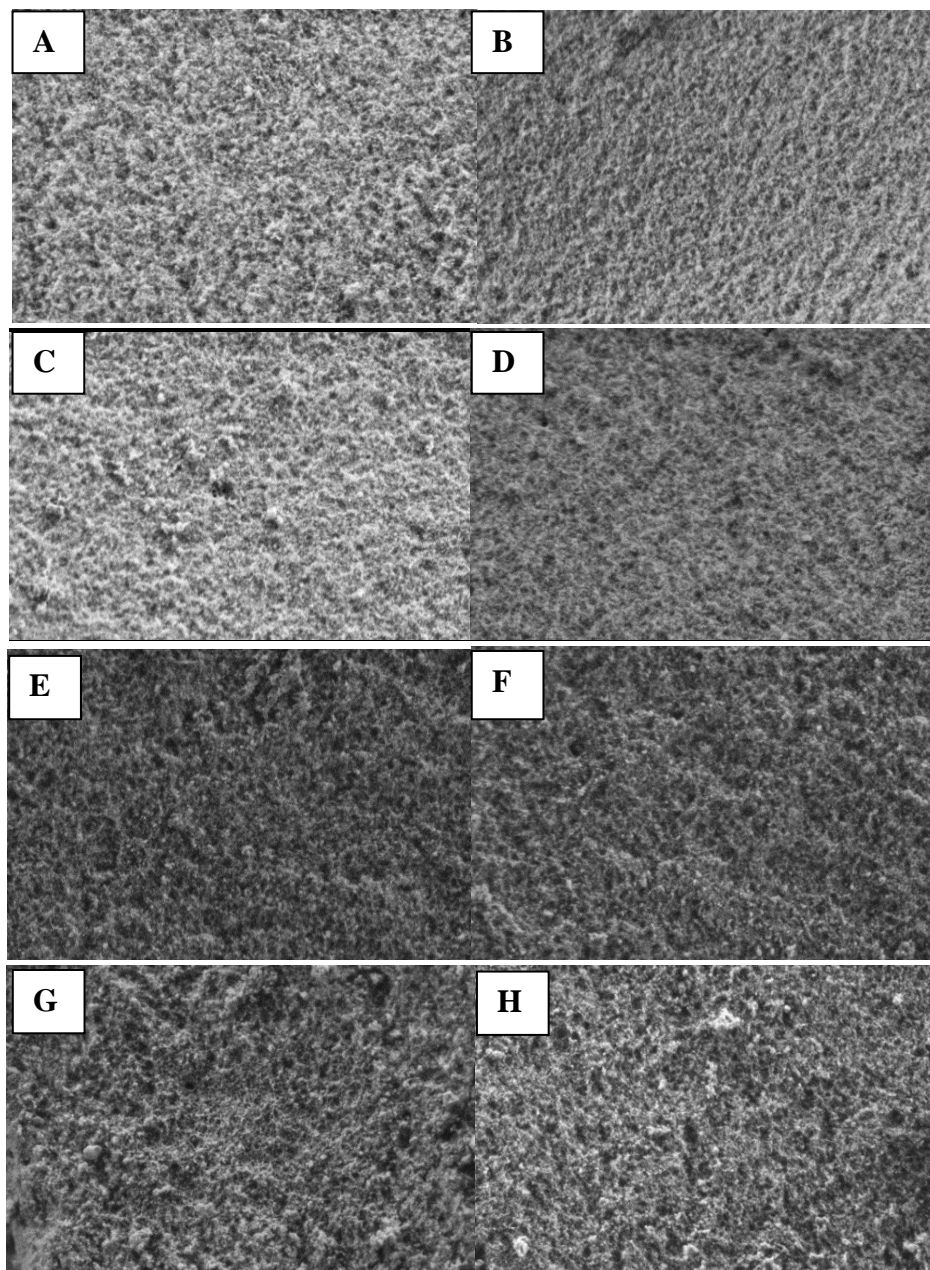
Fig. 7. SEM images of SO_4^{2-}/4ZrKIL-2 (a), SO_4^{2-}/8ZrKIL-2 (b), SO_4^{2-}/15ZrKIL-2 (c), SO_4^{2-}/25ZrKIL-2 (d) samples, and their spent analogues (e-h).

The TEM images (Supplementary data SD1) show that on samples with lower zirconia content no crystalline phases can be detected which is in accordance with XRD data, whereas on the samples with higher zirconia content crystalline zirconia sulfate phases appeared, separately or on the surface of silica carrier.

3.3. Catalytic activity for LA esterification with ethanol and butanol

The samples were investigated in the esterification of levulinic acid with alcohols - ethanol and n-butanol. Non-sulfated Zr-containing KIL-2 samples show very low catalytic activity in esterification reaction with ethanol (not shown). This can be explained by the presence of only Lewis acid sites in the samples. Levulinic ester is the only registered carbon products in the esterification reaction.

The sulfating treatment of the Zr-containing samples leads to a significant increase in the catalytic activity in esterification of levulinic acid with ethanol (Fig. 8). After 5 h reaction time over all samples a conversion of up to 50% is reached and in the next 2 h the catalysts keep the same catalytic activity. When a series of sulfated Zr-KIL-2 was used as catalysts, catalytic activity significantly increased in the order of: $SO_4^{2-}/4ZrKIL-2 < SO_4^{2-}/8ZrKIL-2 < SO_4^{2-}/15ZrKIL-2$, demonstrating that sulfate anions (SO_4^{2-}) act as main active sites for this reaction. The highest catalytic activity was observed for the sulfated 15ZrKIL-2 sample resulting in a conver sion of 51% after 5 h. Further increase of the Zr content leads to a decrease of the catalytic activity.

Table 4 Acidity of the studied samples based on the FT-IR spectra of adsorbed pyridine.

Sample	Py-L (100°C)[a] (1448cm^{-1})	Py-B (100°C)[a] (1548 cm^{-1})	B/L	Py-L (200°C)[a] (1448cm^{-1})	Py-B (200°C)[a] (1548 cm^{-1})	B/L
$SO_4^{2-}/4ZrKIL-2$	0.238	0.063	0.26	0.166	0.033	0.20
$SO_4^{2-}/8ZrKIL-2$	0.160	0.157	0.98	0.222	0.145	0.65
$SO_4^{2-}/15ZrKIL-2$	0.139	0.167	1.20	0.105	0.115	1.09
$SO_4^{2-}/25ZrKIL-2$	0.100	0.205	2.05	0.069	0.097	1.41

[a]mmol acidity calculated with integrated molar extinction coefficients determined by Emeis et al.: 2.22 cmμmol^{-1} for 1448 cm^{-1} band and 1.67 cmμmol^{-1} for 1548 cm^{-1} band and normalized to 5 mg/cm^2 pellet thickness
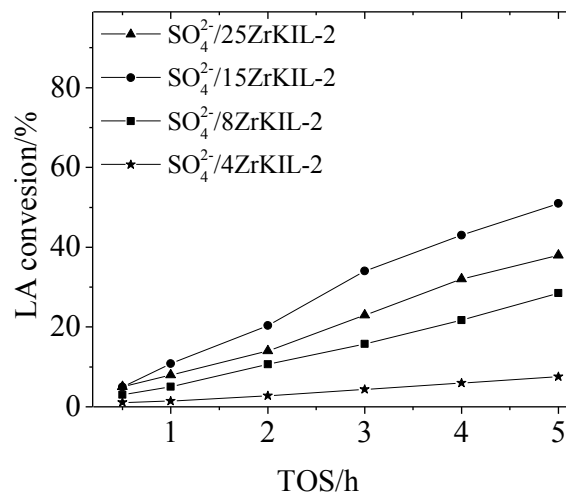
Fig. 8. Conversion of levulinic acid in the esterification of levulinic acid with ethanol as a function of reaction time over different sulfated Zr-KIL-2 catalysts. Reaction temperature =70°C.

One possible reason for the higher activity of the SO_4^{2-}/15ZrKIL-2 sample could be the determined higher density of Brönsted and Lewis acid sites in it than that registered for the SO_4^{2-}/4ZrKIL-2 and SO24/8ZrKIL-2 samples. It could be assumed that the dispersion of the acid sites and the associated accessibility of the organic reactants play an important role in determining the activity [42]. We assumed that the mesoporosity of the silica support assures high dispersion of the acid sites (mainly SO_4^{2-} sites), and this way most of the acid sites become accessible for the reactants. The post synthetic sulfation procedure is more effective for the preparation of active sites with high acid density than the direct sulfation procedure. The former one usually results in the formation of intra-framework SO_4^{2-} species which are not accessible by the reactant molecule [40]. In order to clarify the role of the formed species in the catalytic reaction the spent catalysts were characterized by XRD, N_2 physisorption, SEM and EDX measurements. XRD patterns (Supplementary data, SD2) of the spent sulfated analogues of 4ZrKIL-2 and 8ZrKIL-2 after catalytic reaction show the presence of tetragonal zirconia (4-013-4748), while in sulfated 15Zr/KIL-2 sample monoclinic zirconia and zirconium sulfate tetrahydrate can be found. The sulfated 25Zr/KIL-2 sample shows only the presence of monoclinic and tetragonal zirconia. SEM images of the spent catalysts (Fig. 7g,h) show the presence of crystalline phases (oxide/sulfate) for the SO_4^{2-}/15ZrKIL-2and SO_4^{2-}/25ZrKIL-2 catalysts and only nanoparticles (Fig. 7e, f) of disordered mesoporous KIL-2 silica for the SO_4^{2-}/4ZrKIL-2 and SO_4^{2-}/8ZrKIL-2 samples. A significant decrease of sulfur content (Table 2) was observed for the spent SO_4^{2-}/25ZrKIL-2 sample by EDX method which is due to the leaching of sulfate groups as it was shown by TG analysis as well. However, there is no significant decrease of sulfur content for the sulfate ZrKIL-2 samples with zirconia amount up to 15 wt% (Table 2). The obtained results by EDX for the spent catalysts are in good agreement with the data from XRD, TG analysis and N2 physisorption data.

Table 5 Catalytic activity of the solid catalysts for levulinic acid esterification with ethanol

| Catalyst	Conversion, %	Reaction conditions
Amberlist [4]	55	T = 70°C,
SO_4^{2-}/ZrO_2 [4]	9	5 h reaction time,
SO_4^{2-}/SnO_2 [4]	44	ethanol/LA molar ratio of 5:1,
SO_4^{2-}/SnO_2 [4]	39	2.5 wt.% of catalyst
SO_4^{2-}/Nb_2O_5 [4]	14	
HZSM-5 [4]	5	
PrSO$_3$HSBA-15 [15]	48	T=75°C, 3 h reaction time, ethanol/LA molar ratio of 5:1, 0.072mmol H$^+$/g LA
SO_4^{2-}/Si-ZrO$_2$ (Si/Zr=0.075) [16]	77	T= 70°C, LA:EtOH = 1:10, 10.0 wt.% of catalyst
Keggin HPA [20]	93	T=78°C, 10 h reaction time, ethanol/LA
Wells-Dowson HPA [20]	79	molar ratio of 64:1, 1g catalyst/ 2 mmol LA
Mesoporous H/BEA (Si/Al=10) [23]	40	T=78°C; 5 h reaction time; LA:ethanol molar ratio = 1:6; catalyst loading=20 wt.% of LA
$SO_4^{2-}/15ZrKIL$-2, this study	51(47)	this paper

The comparison of the catalytic activity of the $SO_4^{2-}/15ZrKIL$-2 sample to that of the other solid acid catalyst, i.e. Amberlyst-15, Keggin HPS and Wells-Dowson HPA as reported in literature is presented in Table 5 [4,13,15,16,20,23]. The higher catalytic activity which is observed for SO_4^{2-}/Si-ZrO2, Keggin HPA and Wells-Dowson HPA is due to the higher amount of applied catalyst in the catalytic reaction (Table 5). Only Amberlyst-15 (55% LA conversion after 5 h) shows similar catalytic activity to the $SO_4^{2-}/15ZrKIL$-2 sample at the same reaction conditions [4]. One of the advantages of the sulfated $SO_4^{2-}/15ZrKIL$-2 is its reusability. The $SO_4^{2-}/15ZrKIL$-2 sample shows stable catalytic activity (Table 5), LA conversion is 47% after 3 reaction cycles, compared to the 51% conversion in the first reaction cycle. The reusability and stability of the catalyst are of key importance for practical applications as the life time of the catalysts predetermines the cost of the overall process. The less pronounced leaching of sulfate groups registered on the $SO_4^{2-}/15ZrKIL$-2 sample after the catalytic experiment compared to the other studied samples (Table 2) could be a possible reason for its reusability with only a slight loss in catalytic activity.

The catalytic performance of the sulfated Zr-KIL-2 samples in esterification of levulinic acid with n-butanol at different reaction temperatures is shown in Fig. 9. At a lower reaction temperature (70°C) all samples show much lower catalytic activity than in esterification of LA with ethanol. With the increase of the reaction temperature (100°C) a significant increase of activity can be observed. This effect is more pronounced in the $SO_4^{2-}/15ZrKIL$-2 sample because a significant part of the strong acid sites are deposited into the channels of the KIL-2 matrix.

Disordered mesoporous KIL-2 silica possesses high surface area and relatively large pore sizes assuring high zirconia dispersion for samples with zirconia content up to 15 wt%. The catalytic activity of bulk sulfated ZrO_2 (applied amount correspond to the 15 wt% zirconia in used catalyst in our experiment) in LA esterification is much lower than that of $SO_4^{2-}/15ZrKIL-2$ sample. Moreover the activity of the $SO_4^{2-}/25ZrKIL-2$ sample is lower than that of the $SO_4^{2-}/8ZrKIL-2$ catalyst, whereas at a lower temperature this effect on the catalytic activity is the opposite. The catalytic results can be explained by the most pronounced leaching of the sulfate groups in the $SO_4^{2-}/25ZrKIL-2$ sample (Table 2) and the presence of acid sites with different strength on the studied samples with a different zirconia amount as it was shown by the FT-IR data.

The presence of mesopores and the absence of micropores were determined by nitrogen isotherms of the spent catalysts and textural properties are listed in Table 1. The decrease of total and mesopore volume and surface area of all spent samples can be observed. Pore width distributions are broader and average pore diameters are lower (from 15.9 to 15.3 nm) comparing to samples before the reaction. Spent sulfated 25Zr/KIL-2 sample shows higher specific surface area (270 m^2/g) than its analogue before reaction (139 m^2/g) indicating leaching of zirconium sulfate species from the support, which is in accordance with XRD data.
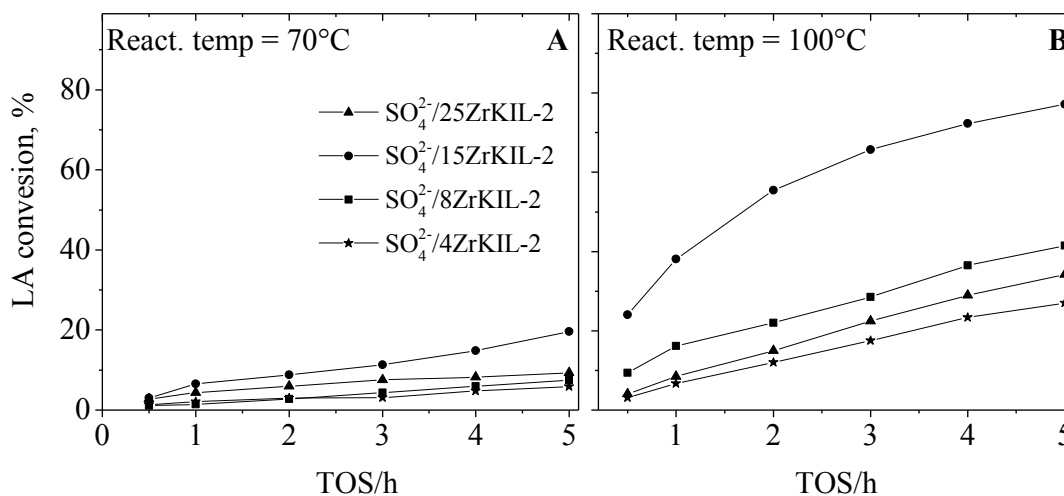
Fig. 9. Conversion of levulinic acid in the esterification of levulinic acid with n-butanol over different sulfated ZrKIL-2 samples at different reaction temperatures: 70°C (A), 100°C (B) as a function of reaction time.

The obtained catalytic data for the activity and stability of the sulfated mesoporous Zr-containing KIL-2 silica materials show that these catalysts can be used as more efficient, reusable and stable solid acid catalysts for the levulinic acid esterification compared to the conventional sulfated zirconia. Despite the fact that a leaching of some fractions of sulfate anions is unavoidable under the reac- tion conditions applied, this process could be minimized by an appropriate ratio of Zr/ SO_4^{2-}.

4. Conclusions

Sulfated zirconia modified mesoporous KIL-2 silicas were pre- pared by incipient wetness impregnation and investigated in levulinic acid esterification with ethanol or n-butanol. The studied catalysts show a high levulinic acid conversion of up to 51% after 5 h. Sulfated materials show significantly higher conversion compared to non-sulfated ones due to their strong Brönsted acidity. It was found that the silica supported sulfated samples show different activity depending on the applied alcohol. The sulfated 15 wt% ZrO2containing KIL-2 catalyst appears to be the most efficient one in the esterification reaction. Further increase of the amount of zirconia leads to activity decrease because of the significant decrease of ZrO2dispersion and the structure deterioration of the catalyst. The investigations of the acidic properties of the sulfated zirconia modified mesoporous KIL-2 silicas revealed that depending on the zirconia amount, acid sites (Brönsted and Lewis) with different strength and distribution were formed. For the first time the sulfate groups leaching were found to depend on the dispersion of zirconia species supported on the mesoporous silica support.

References

[1] R. Luque, J. Campelo, J. Clark, Handbook of Biofuels Production: Processes and Technologies, Woodhead Publishing Series in Energy No. 15, 2013.

[2] C.S.K. Lin, L.A. Pfaltzgraff, L. Herrero-Davila, E.B. Mubofu, S. Abderrahim, J.H. Clark, A. Koutinas, N. Kopsahelis, K. Stamatelatou, F. Dickson, S. Thankappan, Z. Mohamed, R. Brocklesby, R. Luque, Energy Environ. Sci. 6 (2013) 426-464.

[3] J.H. Clark, V. Budarin, Th Dugmore, R. Luque, Catal. Commun. 9 (2008) 1709-1714.

[4] D.R. Fernandes, A.S. Rocha, E.F. Mai, C.J.A. Mota, V. Teixeira da Silva, Appl. Catal. A 425-426 (2012) 199-204.

[5] F.M.A. Geilen, B. Engendahl, A. Harwardt, W. Marquardt, J. Klankermayer, W.Leitner, Angew. Chem. Int. Ed. 49 (2010) 5510-5514.

[6] X.-R. Chen, Y.-H. Ju, C.-Y. Mou, J. Phys. Chem. C 111 (2007) 18731-18737.

[7] A. Corma, S. Iborra, A. Velty, Chem. Rev. 107 (2007) 2411-2502.

[8] A.A. Peterson, F. Vogel, R.P. Lachance, M. Froling,€ M.J. Antal Jr., J.W. Tester, Energy Environ. Sci. 1 (2008) 32-65.

[9] F.D. Pileidis, M. Tabassum, S. Coutts, M.-M. Titirici, Chin. J. Catal. 35 (2014) 929-936.

[10] J.N. Chheda, G.W. Huber, J.A. Dumesic, Angew. Chem. Int. Ed. 46 (2007) 7164-7183.

[11] J. Zakzeski, P.C.A. Bruijnincx, A.L. Jongerius, B.M. Weckhuysen, Chem. Rev. 110 (2010) 3552-3599.

[12] J.-P. Lange, R. Price, P.M. Ayoub, J. Louis, L. Petrus, L. Clarke, H. Gosselink, Angew. Chem. Int. Ed. 49 (2010) 4479-4483.

[13] Y. Kuwahara, T. Fujitani, H. Yamashita, Catal. Today 237 (2014) 18-28.

[14] L. Fuxiang, Y. Feng, L. Yongli, L. Ruifeng, X. Kechang, Micropor. Mesopor. Mater 101 (2007) 250-255.

[15] J.A. Melero, G. Morales, J. Iglesias, M. Paniagua, B. Hernandez, S. Penedo, Appl. Catal. A 466 (2013) 116-122.

[16] Y. Kuwahara, W. Kaburagi, K. Nemoto, T. Fujitani, Appl. Catal. A 476 (2014) 186-196.

[17] S. Dutta, S. De, B. Saha, Biomass bioenergy 55 (2013) 355-369.

[18] S. Bezergianni, A. Dimitriadis, Renew. Sustain. Energy Rev. 21 (2013) 110-116.

[19] G.D. Yadav, A.R. Yadav, Chem. Eng. J. 243 (2014) 556-563.

[20] G. Pasquale, P. Vazquez, G. Romanelli, G. Baronetti, Catal. Commun. 18 (2012) 115-120.

[21] J. Zhang, ShB. Wu, B. Li, H.D. Zhang, ChemCatChem 4 (9) (2012) 1230-1237.

[22] C. Pirez, K. Wilsonc, A.F. Lee, Creen Chem. 16 (2014) 197-202.

[23] C.R. Patil, P.S. Niphadkar, V.V. Bokade, P.N. Joshi, Catal. Commun. 43 (2014) 188-191.

[24] A. Clearfield, G.P.D. Serrette, A.H. Khazi-Syed, Catal. Today 20 (1994) 295-312.

[25] S.-Y. Chen, J.-F. Lee, S. Cheng, J. Catal. 270 (2010) 196-205.

[26] S. Andrizone, C.L. Bianchi, M. Signoretto, Appl. Surf. Sci. 136 (1998) 213-220.

[27] X.-R. Chen, Y.-H. Ju, C.-Y. Mou, J. Phys. Chem. C 111 (2007) 18731-18737.

[28] S. Ardizzone, C. Bianchi, E. Grassi, Colloids Surf. 135 (1998) 41-51.

[29] S. Brunauer, P.H. Emmett, E. Teller, J. Am. Chem. Soc. 60 (1938) 309-319.

[30] K.S.W. Sing, D.H. Everett, R.A. Haul, L. Moscou, R.A. Pirroti, J. Rouquerol, T.Siemieniewska, Pure Appl. Chem. 57 (1985) 603-619.

[31] B.C. Lippens, J.H. de Boer, J. Catal. 4 (3) (1965) 319-323.

[32] E.P. Barrett, L.G. Joyner, P.P. Halenda, J. Am. Chem. Soc. 73 (1951) 373-380.

[33] V.G. Deshmane, Y.G. Adewuyi, Catal. A 462e463 (2013) 196-206.

[34] K. Arata, M. Hino, Mater. Chem. Phys. 26 (1990) 213-237.

[35] M. Popova, A. Szegedi, A. Ristic, N.N. Tusar, Catal. Sci. Technol. 4 (2014) 3993-4000.

[36] R. Barthos, F. Lonyi, J. Engelhardt, J. Valyon, Top. Catal. 10 (2000) 79-87.

[37] C. Morterra, G. Cerrato, V. Bolis, Catal. Today 17 (1993) 505-515.

[38] C. Morterra, G. Cerrato, C. Emanuel, V. Bolis, J. Catal. 142 (1993) 349-367.

[39] E.E. Platero, M.P. Mentruit, C.O. Arean, A. Zecchina, J. Catal. 162 (1996) 268-276.

[40] K. Barbera, P. Lanzafame, A. Pistone, S. Millesi, G. Malandrino, A. Gulino, S. Perathoner, G. Centi, J. Catal. 323 (2015) 19-32.

[41] M.A. Ecormier, K. Wilson, A.F. Lee, J. Catal. 215 (1) (2003) 57-65.

[42] K. Wilson, A.F. Lee, D.J. Macquarrie, J.H. Clark, Catal. A 228 (2002) 127-133.